HHS Public Access

Author manuscript

Alzheimers Dement. Author manuscript; available in PMC 2021 March 01.

Published in final edited form as:

Alzheimers Dement. 2020 March ; 16(3): 561–571. doi:10.1016/j.jalz.2019.09.079.

Tau-PET Correlates with Neuropathology Findings

Val J. Lowe, MD[1], **Emily S. Lundt, MS**[2], **Sabrina M. Albertson, BS**[2], **Hoon-Ki Min, PhD**[1], **Ping Fang, MS**[1], **Scott A. Przybelski, BS**[2], **Matthew L. Senjem, MS**[3], **Christopher G. Schwarz, PhD**[1], **Kejal Kantarci, MD**[1], **Bradley Boeve, MD**[4], **David T. Jones, MD**[4], **R. Ross Reichard, MD**[5], **Jessica F. Tranovich, BS**[6], **Fadi S. Hanna Al-Shaikh, BS**[6], **David S. Knopman, MD**[4], **Clifford R. Jack Jr., MD**[1], **Dennis W. Dickson, MD**[6,7], **Ronald C. Petersen, MD, PhD**[4], **Melissa E. Murray, PhD**[6]

[1]Department of Radiology, Mayo Clinic, Rochester MN

[2]Department of Health Sciences Research, Mayo Clinic, Rochester MN

[3]Department of Information Technology, Mayo Clinic, Rochester MN

[4]Department of Neurology, Mayo Clinic, Rochester MN

[5]Department of Laboratory Medicine & Pathology, Mayo Clinic, Rochester MN

[6]Department of Neuroscience, Mayo Clinic, Jacksonville, Florida

[7]Department of Laboratory Medicine & Pathology, Mayo Clinic, Jacksonville, Florida

Abstract

INTRODUCTION: Comparison of tau (flortaucipir) positron emission tomography (FTP-PET) to autopsy is important to demonstrate the relationship of FTP-PET to neuropathologic findings.

METHODS: Autopsies were performed on 26 participants who had antemortem FTP-PET. FTP-PET standardized uptake value ratios (SUVr) were compared to autopsy diagnoses and Braak tangle stage. Quantitative tau burden was compared to regional FTP-PET signal.

RESULTS: Participants with Braak stages of IV or greater had elevated FTP-PET signal. FTP-PET was elevated in participants with Alzheimer's disease. An FTP-PET SUVr cut-point of 1.29 was determined to be optimal. Quantitative measurements of hippocampal and temporal lobe tau burden were highly correlated to FTP-PET signal (rho's from 0.61 to 0.70, $p \leq 0{,}002$).

CONCLUSIONS: Elevated FTP-PET reflects Braak IV or greater neuropathology. Participants with primary age-related tauopathy and hippocampal sclerosis did not show elevated FTP-PET signal. Secondary neuropathologic diagnoses of Alzheimer's disease neuropathologic change can lead to borderline elevated FTP-PET signal.

Corresponding Authors: Val J. Lowe, MD, Department of Radiology, CH 1-285, Mayo Clinic, 200 First Street SW, Rochester, MN 55905 USA, Telephone: 507 284-4104, vlowe@mayo.edu; Melissa E. Murray, PhD, Department of Neuroscience, 4500 San Pablo Road South, Mayo Clinic, Jacksonville, FL 32224 USA, Telephone: 904-953-1083, murray.melissa@mayo.edu.

1.0 Introduction

Post-mortem studies in Alzheimer's disease (AD) have classified six consecutive Braak tangle stages describing the regional deposition of hyperphosphorylated tau protein over the course of the disease [1, 2]. Braak tangle staging is strongly associated with cognitive impairment [1, 3–6] and is a core element of the neuropathologic features of the diagnosis of AD [7, 8].

Tau positron emission tomography (tau-PET) imaging allows study of tau neuropathology *in vivo* [9–11] and initial studies have shown that tau-PET correlates with AD neurofibrillary tangles *in vitro* [12]. In aging, tau-PET signal has been described to occur in the medial temporal lobe as well as in extra-temporal areas of the brain [13] and increases in these regions in longitudinal studies [14].

The composition of fibrillar tau differs across tauopathies, [15] engendering challenges for tau-PET imaging. PET imaging with flortaucipir (FTP) has shown highly sensitive binding affinity to tau in AD patients [16, 17]. FTP "off-target" binding has been reported in entities not considered to be associated with tau accumulation such as neuromelanin and the choroid plexus [12, 18]. To date only single case studies of *in vivo* tau-PET compared to autopsy in various tauopathies have been reported [18–21]. Of these, one postmortem AD case with correlation with FTP-PET has been published [22]. Validating FTP-PET binding with neuropathology is important and more data is needed to rigorously assess the utility of this technology. Therefore, our goals were to: 1) evaluate the association of FTP-PET and neuropathologic diagnoses at autopsy; 2) evaluate the association of FTP-PET and Braak tangle stage at autopsy; and 3) compared regional quantitative FTP-PET findings to quantitative immunohistochemistry.

2.0 Materials and Methods

2.1 Participants

Participants were part of the Mayo Clinic Study of Aging (MCSA) or Mayo Clinic Alzheimer's Disease Research Center (ADRC) as described previously [14]. All participants or designees provided written consent with approval of Mayo Clinic and Olmsted Medical Center Institutional Review Boards. There were 1293 participants enrolled between April, 2015 and September, 2018. 28 who died sequentially in this group were eligible for evaluation. Of these, 26 had full clinical evaluations including cognitive assessments, FTP-PET and MRI within 3 years of death (average 15 months) and complete neuropathologic evaluations. Antemortem clinical information including age of onset of cognitive symptoms, education, and Mini-Mental State Examination (MMSE) score [23] were assessed in all 26 during study visits. The MMSE and clinical data at the time of last imaging prior to death were used in statistical analyses. 8/26 participants were too impaired to complete MMSE in conjunction with the imaging testing most proximal to death, and in these, MMSE data available from the most recent prior visit was reported. All cognitive tests were administered by experienced psychometrists and supervised by board certified clinical neuropsychologists. Categorical clinical diagnoses are described in the supplemental materials (Supplemental Methods).

2.2 Neuroimaging methods

PET/CT was performed and regionally assessed as reported previously [13] (see supplemental methods). FTP-PET data with and without partial volume correction (PVC) employing the two compartment method were obtained as previously described [24]. Amyloid PET imaging with Pittsburgh compound B (PiB) as previously described [25] was available for descriptive comparison on all but one of the AD participants.

Median SUVr values from ROIs in each participant's MRI atlas template were extracted. Analysis was performed on an FTP-PET meta-ROI that has previously been shown to accurately capture within subject tau signal for longitudinal evaluation and have a broad dynamic range across the normal to pathological aging to AD dementia spectrum [14, 26]. This meta-ROI included the amygdala, entorhinal cortex, fusiform, parahippocampal, and inferior temporal and middle temporal gyri. Analysis of entorhinal cortex as a single ROI was also performed. The FTP-PET ROI median values were normalized to cerebellar crus (bilateral crus, 1-2) to calculate regional standardized uptake value ratios (SUVr)[13]. Data with and without partial volume correction (PVC) were evaluated. Correlative analysis of quantitative immunohistochemistry (IHC) and regional FTP-PET signal was performed in three ROIs defined by the MRI brain atlas (hippocampus, middle temporal, and superior temporal) that were sites of probable early tau involvement, were all sampled at autopsy, and were included in an automated image/autopsy-tissue correlation program we previously developed [27]. These ROIs were side-matched to respective tissue regions sampled.

To assess the correlation of different regional PET analysis methods with neuropathology, separate descriptive analyses were done for FTP-PET with cortical gray matter (GM) or gray matter plus white matter (GM+WM) region sampling; and with or without partial volume correction. Imaging correlation to neuropathologic schemes was done for the FTP-PET meta-ROI and entorhinal cortex ROI.

2.3 Neuropathology methods

Standardized neuropathologic examination and brain sampling was performed according to the CERAD protocol[28]. Tissue samples were paraffin-embedded and routinely stained with hematoxylin and eosin and a modified Bielschowsky silver stain. Immunohistochemistry was performed using antibodies to phospho-tau (AT8;1:1000; Endogen, Woburn, MA), Aβ (6F/3D;1:10; Novocastra VectorLabs, Burlingame, CA), and α-synuclein (LB509;1:200 dilution; Zymed, San Francisco,CA). Using recommendations from the National Institute on Aging-Alzheimer's Association (NIA-AA) guidelines [7, 8], the AT8 immunostained sections were used to assess Braak tangle stage and neuritic plaque score. Argyrophilic grains were detected with Bielschowsky and AT8 immunohistochemistry, supplemented by 4R tau immunohistochemistry, as needed. Aβ immunohistochemistry in the neocortex, hippocampus, basal ganglia and cerebellum was used to assign Thal amyloid phase as: Phase 1- neocortex; Phase 2-CAI/subiculum; Phase 3-basal ganglia or dentate fascia of the hippocampus; Phase 4–midbrain or CA4 of the hippocampus; and Phase 5-cerebellum. The presence of cerebrovascular disease was assessed by presence of white matter rarefaction or cribriform change in the basal ganglia, or both, in association with marked arteriolosclerosis or atherosclerosis, with or without

presence of microinfarcts, lacunar (<1-cm) infarcts, or larger infarcts. *APOE* genotyping was performed antemortem from DNA extracted from blood samples according to standard protocols.

Participants were assigned the neuropathologic diagnosis of AD if they had a Braak tangle stage of ≥ IV and had at least a moderate neuritic plaque score. Participants were defined as pathological aging [29] (also referred to as Alzheimer changes insufficient to diagnose AD) if they had a Braak tangle stage of III or less, at least a moderate diffuse plaque score, and no more than a moderate neuritic plaque score. Cases were defined as senile change if they had a Braak tangle stage of III or less, at least sparse diffuse plaques, and no neuritic plaques. To facilitate translation of our findings, senile change and pathological aging cases were re-assigned as primary age-related tauopathy (PART) if they met published criteria – Braak tangle stage I-IV and Thal amyloid phase 2 or less[30]. Definite PART was defined by Thal amyloid phase 0, whereas probable PART cases could have some amyloid pathology present (Thal phase 1–2). Frontotemporal lobar degeneration with TDP-43 [31] corticobasal degeneration (CBD) [32], progressive supranuclear palsy [33], and globular glial tauopathy (GGT) [34] were diagnosed according to recommended criteria. Lewy body disorders were classified neuropathologically based on the distribution and severity of Lewy bodies and neurites as: diffuse (neocortical) (DLBD), transitional (Limbic) (TLBD), brainstem-predominant (BLBD), amygdala-predominant (ALB), or olfactory bulb only, according to standard criteria [35, 36]. Hippocampal sclerosis of a TDP-43 etiology was diagnosed as previously described [37].

We utilized a research-based rubric that balances severity, commonality and rarity of a disorder, without influence of the clinical phenotype to determine primary and secondary pathology. For example, advanced AD pathology takes precedent over co-existing α-synucleinopathies. Milder AD pathology, however, would be secondary to a more severe presentation of an α-synucleinopathy – an example would be participant #22. Vascular disease would be secondary to a more advanced presentation of AD pathology. However, primary tauopathies, which rarely coincide with advanced AD are considered as primary. Common age-related tauopathies are considered as secondary, as these are considered a co-existing pathology.

Quantitative analysis of immunohistochemical tau burden was performed using digital pathology methods. PHF-1 was previously identified to relate more closely to FTP autoradiographic binding than CP13, which is a phospho-tau antibody similar in profile to AT8 [12]. Thus, we additionally performed PHF-1 immunohistochemistry (1:1000 mouse monoclonal anti-phospho-serine 396/404 tau, from Peter Davies) on the temporal cortex (middle and superior) and posterior hippocampus for quantitative tau burden measurement. Slides were scanned using the high-throughput ScanScope AT2 (Leica Biosystems, Buffalo Grove, IL). Slides were annotated using ImageScope software (Leica Biosystems, Buffalo Grove, IL) and analyzed using a custom-designed color deconvolution macro. The output was a percentage of immunopositive staining per area traced to represent the percent tau burden for each tissue region.

2.4 Statistical Analyses

Correlations between SUVr in the FTP-PET meta-ROI and Braak tangle stage were computed using Spearman's rank correlation coefficient (rho). A similar analysis was performed for entorhinal cortex. An ROC analysis was performed on meta-ROI and entorhinal FTP-SUVr to identify the optimal cut-point for separating AD spectrum diagnosis (AD/PA) as a primary or secondary pathology diagnosis from the non-AD spectrum neuropathologic diagnoses [38]. The optimal cut-point was identified as the point maximizing the Youden function which is the difference between the true positive (TPR) and false positive rate (FPR) over all possible cut-point values [39]. A 95% confidence interval on the cut-points were computed using 2000 stratified bootstrap replicates. Sensitivity and specificity with 95% confidence intervals were computed to assess the performance of the cut points.

Tau percent burden from IHC quantification was correlated to FTP-PET SUVr measures using Spearman's rank correlation coefficient (rho). Hippocampus, middle temporal, and superior temporal regions were used in the IHC correlation. Scatterplots between SUVr and tau burden were constructed and included local regression curves with 95% confidence bands (shaded). Local regression was used as a non-parametric approach for generating smooth curves by fitting multiple regressions in a local neighborhood points (x,y) where x is SUVr and y is tau burden (%PHF-1).

All analyses were performed using R Statistical Software (v3.4.1) employing the pROC package for ROC analyses.

3.0 Results

3.1 FTP-PET Imaging and Autopsy Participants

The participant demographics by neuropathologic diagnoses are shown in Table 1. Individual participant data are shown in Table 2. Autopsy diagnoses included AD (n=11, participants 1-11), pathological aging (n=1, participant 12), globular glial tauopathy (n=1, participant 13), PART (n=3, participants 14-16), LBD (n=9, participants 17-25), and hippocampal sclerosis-TDP (n=1, participant 26). There were 16 men and 10 women. While 8 participants were clinically normal, all participants had some detectable neuropathology. The primary neuropathologic diagnoses considered to be in the AD spectrum were AD and pathological aging. AD participants had more severe cognitive deficits (average MMSE 18) and all had abnormal amyloid PET.

3.2 *FTP-PET* Relationship to *Autopsy Diagnosis and Braak NFT stage*

The distribution of SUVr for different primary neuropathologic diagnoses is shown in Fig. 1. We determined that the optimal meta-ROI and entorhinal tau SUVr cut-points were 1.29 (bootstrap confidence interval of 1.28, 1.40) and 1.27 (bootstrap confidence interval of 1.22, 1.41) respectively when analyzing the data in gray and white matter (GMWM) and with no partial volume correction. This optimal meta-ROI threshold had a sensitivity and specificity of 87% and 82% to identify AD-spectrum primary or secondary diagnoses (Supplemental Table 1). Those with Braak tangle stages of IV or greater were all FTP-PET positive based

on a threshold of 1.29 (Fig. 2). Performing the same comparisons using only the entorhinal cortex produced very similar results (Supplemental Figure 1 **and** Figure 2). The cut-point varied minimally when using partial volume correction or GM only (Supplemental Table 1). All participants in the AD spectrum had an abnormal SUVr except for the pathological aging participant. The AD participant with the lowest tau SUVr (1.3) was considered positive at the threshold of 1.29 while the PART participants were negative(SUVr values of 1.27, 1.25, and 1.14). LBD participants were sometimes FTP-PET positive (3/9). The hippocampal sclerosis-TDP participant (SUVr of 1.26) was negative at the optimal threshold. Participants with no primary neuropathologic diagnosis of AD that had elevated FTP-PET signal sometimes had a secondary neuropathologic diagnoses in the AD spectrum. This included participant 22 (TLBD) with a secondary neuropathologic diagnoses of AD and participant 18 (DLBD) with a secondary diagnosis of pathological aging (SUVr of 1.37 for both). Participant 13 with an SUVr of 1.39 had a GGT primary diagnosis (Braak 0) and a secondary diagnosis of HpScl-TDP. FTP-PET signal elevation in this case represented FTP uptake in 4R tau (Supplemental Figure 3). A DLBD participant with a secondary diagnosis of senile change had an SUVr of 1.37 (participant 17). The sole participant with a *primary* neuropathologic diagnosis of pathological aging (Braak I) and had an FTP-PET SUVr of 1.15.

3.3 FTP-PET correlation with quantitative tau IHC measurement

Quantitative histologic analyses demonstrated moderately strong correlations between FTP-PET SUVr in temporal regions (hippocampus, middle temporal and superior temporal) compared to quantitative measurement of tau burden (Fig. 3 A; rho's from 0.61-0.70, $p \leq 0.002$). Several of the tissue samples had a tau burden in the range of 5% or less. To facilitate interpretation, we provided graphical analyses using both raw (Fig. 3 A) and log scale (Fig. 3 B) to give a descriptive sense of the relationship with low tau.

3.4 FTP-PET Image Examples

FTP-PET image examples of AD, Pathological Aging, PART, GGT, DLBD, and Hippocampal Sclerosis are show in Fig. 4. An AD participant who had an abnormal, but lower-range, SUVr of 1.3 is shown. Visually the images in this participant showed elevated temporal FTP-PET signal and also subtle FTP-PET signal in the parietal-occipital region. The visual findings in these participants in large part confirm the SUVr findings. The participants with PART had non-elevated SUVr values (1.27, 1.25, 1.14) using the meta ROI or by using the entorhinal cortex alone (Supplemental Figure 1). However, visually there was FTP-PET signal in participant #14 (Braak III) in the entorhinal region and middle temporal region (Fig. 4). A participant with DLBD, who had an elevated FTP-PET SUVr of 1.37, showed elevated FTP-PET signal in temporal, posterior cingulate and parietal-occipital regions, of which the latter two may be more typical for LBD tau distribution but would not be captured in the meta-region ROI. FTP-PET signal was focally elevated in the hippocampal sclerosis participant in the right temporal region which was not the side evaluated at autopsy. The GGT case showed elevated focal tau accumulation in temporal and frontal lobes with involvement of white matter.

4.0 Discussion

We evaluated the association of FTP-PET and neuropathologic findings in this work and made several observations. First, positive FTP-PET signal in an AD composite meta-ROI reflects Braak NFT stage IV or greater. Second, participants with LBD plus AD or GGT had elevated tau signal in the AD-centric meta-ROI but the signal intensity was low (not greater than SUVr of 1.5 in this group). Third, the participants with PART, hippocampal sclerosis-TDP, and pathologic aging had non-elevated signal. Fourth, quantitative measurement of tau burden at autopsy and FTP-PET signal are highly correlated.

We showed high correlation of FTP-PET with Braak tangle stage. Our findings are consistent with prior tissue autoradiography data that showed an association of FTP-PET with paired helical filament tau as seen in AD [12, 40]. Smith and colleagues described one participant with AD in which tau-PET during life correlated with findings of regional *in vivo* uptake. They found a correlation between the density of tau-positive neurites, intrasomal tau, and total tau burden with FTP-PET signal (AT8: rs = 0.84; P < .001; Gallyas: rs = 0.82; P < 0.001). No correlations between FTP-PET and beta-amyloid pathology were found [22]. Our findings confirm these prior correlations of tau burden and FTP-PET signal.

Data from non-AD participants with FTP-PET and autopsy correlation have been previously published. A previous report by Marquie, et al, quantified *in vivo* retention of FTP-PET vs. autoradiography, binding assays, and quantitative tau measurements in postmortem brain samples from two progressive supranuclear palsy cases and a *MAPT* P301L mutation carrier. They concluded that FTP-PET has limited utility for *in vivo* selective and reliable detection of tau aggregates in these non-Alzheimer tauopathies [21]. The imaging-postmortem correlation analysis in a Parkinson's disease case demonstrated strong FTP-PET affinity for neurofibrillary tau pathology but also for off-target binding to neuromelanin and blood components [18]. A sporadic Creutzfeldt-Jakob disease (CJD) case showed no unique pattern of FTP-PET by visual inspection or SUVr (1.17, 1.08-1.36) again suggesting that FTP-PET has better specificity for the paired helical tau filaments associated with AD dementia [20]. One group assessed tau-PET using (18)F-THK5351 in an autopsy-confirmed AD patient and regional *in vivo* retention was significantly correlated with the density of tau aggregates in the neocortex and monoamine oxidase-B in the whole brain, but not with insoluble amyloid-beta [19]. Josephs and colleagues showed that FTP-PET signal correlates with 4R tauopathy in a case of CBD [41]. In our cohort, one participant had GGT, a 4R tauopathy, and unexpected elevated FTP-PET signal was seen in the range of what is seen with AD 3R+4R tau. This participant had both co-existing HpScl-TDP and pathological aging and while no neuritic plaques were observed on tau immunostained sections, some cored plaques were observed. An interesting feature in this participant was also extensive white matter tau pathology (Supplemental Figure 3) that was greater than gray matter tau pathology. This was reflected by prominent white matter FTP-PET signal. Whether elevated FTP-PET signal will be a consistent feature in future GGT participants is uncertain.

Histologic quantification has been challenging for many as highlighted by the CERAD group where preference was given to semiquantitative/descriptive measures to assess tissue findings because quantitative measures were found to be "problematic" [42]. Variation in

brain tissue position seen by *in vivo* imaging vs. tissue sampling at autopsy make precise anatomic correlation with images challenging. Nevertheless, we observed a moderately high correlation of quantitative neurofibrillary tangle data and FTP-PET. The data show limitations of the biomarker correlations for low levels, <10%, of tau neuropathology.

The present study was conducted in a population sample and with additional participants included from a clinical referral research center studying early dementia development (ADRC). As a result, many (9/26, see Table 2) were cognitively unimpaired or had MCI at the time of their FTP-PET imaging. This participant group provided a unique view of neuropathologic entities like PART, hippocampal sclerosis and pathological aging. FTP-SUVr values were near the threshold in these entities. None of the scans were performed greater than 2 years before death in the PART participants. The hippocampal sclerosis and pathological aging diagnosis participants died less than a year after imaging. Therefore, any substantial changes in FTP-PET signal in these short time frames is unlikely (approximately 0.5% per year, [14]). In the PART participants, the SUVr values from the meta-ROI or entorhinal cortex ROI did not reach the optimal cut-point value. In one PART participant with the highest Braak stage (#14), focal FTP-PET signal could be seen on visual inspection in the entorhinal cortex and temporal lobe. This suggests that ROI methods may not detect subtle FTP-PET signal in early tau deposition. In hippocampal sclerosis-TDP, our observations were consistent with prior studies showing mild FTP-PET signal (probably "off-target") in clinically suspected TDP participants [12]. These data as a whole would argue against FTP-PET as a reliable clinical measure of such pathology using the cut-point as defined. Further work in a larger group with early tau neuropathological findings needs to address the possibility that sub-threshold elevations of FTP-PET signal, visual assessment, or regional sub-selective analyses may be better in characterizing early pathology.

We paid special attention to mixed pathology given its common presentation at autopsy. Some participants in the group without AD as a primary neuropathological diagnosis had minimally elevated FTP-PET signal likely due to mixed AD pathology. To be sure, a judgment about what is "primary" and what is "secondary" could be seen as somewhat arbitrary. This was highlighted by the LBD participants where we considered the LB pathology to be primary when the AD pathology appeared to be early. Adding other disease biomarkers such as FDG-PET could clarify the diagnosis of these patients for clinical characterization during life [43].

4.1 Study limitations

This study obtained autopsy results not more than three years after FTP-PET but It is possible that the tau burden could have increased in some participants between the scan and death. Our ability to refine the FTP-PET cut-point for individual neuropathologic categorizations was challenged by low numbers in some disease categories, such as PART. FTP-PET signal in off-target sites could be a limitation in some of our analyses. For example, retention in the choroid plexus could bias medial temporal lobe regional findings like the hippocampus, but we found that quantitative IHC correlated well, suggesting that the choroid plexus off-target signal "bleed in" is likely of limited importance.

4.2 Summary

This study showed that tau-PET using FTP is a reliable biomarker of underlying neurofibrillary tangle pathology, as measured by disease diagnosis at autopsy, Braak tangle stage and quantitative IHC. It demonstrated that FTP-PET is well suited to monitor tau burden in AD and may assist in therapeutic clinical trials. The finding that the Braak tangle stage scheme was highly correlated with FTP-PET signal helped to validate FTP-PET as a biomarker for AD.

Supplementary Material

Refer to Web version on PubMed Central for supplementary material.

Acknowledgements:

We thank the patients and their families who have participated in these prospective clinical and imaging studies, and especially for the generous donation of their brain tissue to help further our knowledge in Alzheimer's disease. The authors would like to acknowledge the continuous commitment and teamwork offered by Mark Jacobsen, Ping Fang, Ariston Librero, Virginia R. Phillips, and Monica Castanedes-Casey. We would like to also thank Kris Johnson for assistance in collection of neuropathologic material. We would like to greatly thank AVID Radiopharmaceuticals, Inc., for their support in supplying the F18-flortaucipir precursor, chemistry production advice and oversight, and FDA regulatory cross-filing permission and documentation needed for this work.

6.0 Funding:

This research was supported by NIH grants, P50 AG016574, R01 NS89757, R01 NS089544, R01 DC10367, R01 AG011378, R01 AG041851, R01 AG034676, R01 AG054449, R01 NS097495, U01 AG006786, R21 NS094489, by the Robert Wood Johnson Foundation, The Elsie and Marvin Dekelboum Family Foundation, the Liston Family Foundation and by the Robert H. and Clarice Smith and Abigail van Buren Alzheimer's Disease Research Program, the Alexander Family Foundation, the GHR Foundation, Dr. Corinne Schuler and the Mayo Foundation for Medical Education and Research.

Disclosures/Potential Conflicts of Interest:

Dr. Lowe serves is a consultant for Bayer Schering Pharma, Philips Molecular Imaging, Piramal Imaging and GE Healthcare and receives research support from GE Healthcare, Siemens Molecular Imaging, AVID Radiopharmaceuticals, the NIH (NIA, NCI), and the MN Partnership for Biotechnology and Medical Genomics.

Ms. Lundt reports none.

Ms. Albertson reports none.

Dr. Min reports none.

Mr. Przybelski reports none.

Mr. Weigand reports none.

Mr. Senjem reports none.

Dr. Schwarz receives research support from the NIH.

Dr. Parisi reports none.

Dr. Kantarci serves on the data safety monitoring board for Pfizer Inc and Jannsen Alzheimer's Immunotherapy; data safety monitoring board for Takeda Global Research & Development Center, Inc. She is funded by the NIH and Minnesota Partnership for Biotechnology and Medical Genomics.

Dr. Boeve has served as an investigator for clinical trials sponsored by Axovant and Biogen. He receives royalties from the publication of a book entitled Behavioral Neurology Of Dementia (Cambridge Medicine, 2009, 2017). He

serves on the Scientific Advisory Board of the Tau Consortium. He receives research support from the NIH, the Mayo Clinic Dorothy and Harry T. Mangurian Jr. Lewy Body Dementia Program and the Little Family Foundation.

Dr. Jones reports no disclosures.

Dr. Reichard reports no disclosures.

Mrs Tranovich reports no disclosures.

Mr. Al-Shaikh reports no disclosures.

Dr. Knopman serves on a Data Safety Monitoring Board for the DIAN study; is an investigator in clinical trials sponsored by, Lilly Pharmaceuticals, Biogen and the Alzheimer's Treatment and Research Institute at the University of Southern California; and receives research support from the NIH.

Dr. Jack serves on a scientific advisory board for Eli Lilly & Company and on an independent data safety monitoring board for Roche but he recives no personal compensation from any commercial entity. He receives research support from the NIH, and the Alexander Family Alzheimer's Disease Research Professorship of the Mayo Clinic.

Dr. Dickson reports none

Dr. Petersen serves on scientific advisory boards for Roche, Inc.; Merck, Inc.; Biogen, Inc.; Eisai, Inc.; conducted a CME course for GE Healthcare and is on a DSMB for Genentech, Inc.; receives royalties from the publication of *Mild Cognitive Impairment* (Oxford University Press, 2003); and receives research support from the NIH /NIA.

Dr. Murray receives research support from the NIH/NIA.

7.0 References:

[1]. Braak H, Braak E. Neuropathological stageing of Alzheimer-related changes. Acta Neuropathol. 1991;82:239–59. [PubMed: 1759558]

[2]. Braak H, Alafuzoff I, Arzberger T, Kretzschmar H, Del Tredici K. Staging of Alzheimer disease-associated neurofibrillary pathology using paraffin sections and immunocytochemistry. Acta Neuropathol. 2006;112:389–404. [PubMed: 16906426]

[3]. Bennett DA, Schneider JA, Wilson RS, Bienias JL, Arnold SE. Neurofibrillary tangles mediate the association of amyloid load with clinical Alzheimer disease and level of cognitive function. Arch Neurol. 2004;61:378–84. [PubMed: 15023815]

[4]. Duyckaerts C, Bennecib M, Grignon Y, Uchihara T, He Y, Piette F, et al. Modeling the relation between neurofibrillary tangles and intellectual status. Neurobiol Aging. 1997;18:267–73. [PubMed: 9263190]

[5]. Nelson PT, Alafuzoff I, Bigio EH, Bouras C, Braak H, Cairns NJ, et al. Correlation of Alzheimer disease neuropathologic changes with cognitive status: a review of the literature. J Neuropathol Exp Neurol. 2012;71:362–81. [PubMed: 22487856]

[6]. Sabbagh MN, Cooper K, DeLange J, Stoehr JD, Thind K, Lahti T, et al. Functional, global and cognitive decline correlates to accumulation of Alzheimer's pathology in MCI and AD. Current Alzheimer research. 2010;7:280–6. [PubMed: 19715548]

[7]. Montine TJ, Phelps CH, Beach TG, Bigio EH, Cairns NJ, Dickson DW, et al. National Institute on Aging-Alzheimer's Association guidelines for the neuropathologic assessment of Alzheimer's disease: a practical approach. Acta Neuropathol. 2012;123:1–11. [PubMed: 22101365]

[8]. Hyman BT, Phelps CH, Beach TG, Bigio EH, Cairns NJ, Carrillo MC, et al. National Institute on Aging-Alzheimer's Association guidelines for the neuropathologic assessment of Alzheimer's disease. Alzheimers Dement. 2012;8:1–13. [PubMed: 22265587]

[9]. Zimmer ER, Leuzy A, Gauthier S, Rosa-Neto P. Developments in Tau PET Imaging. The Canadian journal of neurological sciences. 2014;41:547–53. [PubMed: 25424608]

[10]. Hashimoto H, Kawamura K, Igarashi N, Takei M, Fujishiro T, Aihara Y, et al. Radiosynthesis, photoisomerization, biodistribution, and metabolite analysis of 11C-PBB3 as a clinically useful PET probe for imaging of tau pathology. J Nucl Med. 2014;55:1532–8. [PubMed: 24963128]

[11]. Fawaz MV, Brooks AF, Rodnick ME, Carpenter GM, Shao X, Desmond TJ, et al. High affinity radiopharmaceuticals based upon lansoprazole for PET imaging of aggregated tau in Alzheimer's disease and progressive supranuclear palsy: synthesis, preclinical evaluation, and lead selection. ACS Chem Neurosci. 2014;5:718–30. [PubMed: 24896980]

[12]. Lowe VJ, Curran G, Fang P, Liesinger AM, Josephs KA, Parisi JE, et al. An autoradiographic evaluation of AV-1451 Tau PET in dementia. Acta neuropathologica communications. 2016;4:58. [PubMed: 27296779]

[13]. Lowe VJ, Wiste HJ, Senjem ML, Weigand SD, Therneau TM, Boeve BF, et al. Widespread brain tau and its association with ageing, Braak stage and Alzheimer's dementia. Brain : a journal of neurology. 2018;141:271–87. [PubMed: 29228201]

[14]. Jack CR Jr, Wiste HJ, Schwarz Cg, Lowe VJ, Senjem ML, Vemuri P, et al. Longitudinal tau PET in ageing and Alzheimer's disease. Brain : a journal of neurology. 2018;141:1517–28. [PubMed: 29538647]

[15]. Murray ME, Kouri N, Lin WL, Jack CR Jr., Dickson DW, Vemuri P. Clinicopathologic assessment and imaging of tauopathies in neurodegenerative dementias. Alzheimers Res Ther. 2014;6:1. [PubMed: 24382028]

[16]. Chien DT, Bahri S, Szardenings AK, Walsh JC, Mu F, Su MY, et al. Early clinical PET imaging results with the novel PHF-tau radioligand [F-18]-T807. J Alzheimers Dis. 2013;34:457–68. [PubMed: 23234879]

[17]. Xia CF, Arteaga J, Chen G, Gangadharmath U, Gomez LF, Kasi D, et al. [(18)F]T807, a novel tau positron emission tomography imaging agent for Alzheimer's disease. Alzheimer's & dementia : the journal of the Alzheimer's Association. 2013.

[18]. Marquie M, Verwer EE, Meltzer aC, Kim SJW, Aguero C, Gonzalez J, et al. Lessons learned about [F-18]-AV-1451 off-target binding from an autopsy-confirmed Parkinson's case. Acta Neuropathol Commun. 2017;5:75. [PubMed: 29047416]

[19]. Harada R, Ishiki A, Kai H, Sato N, Furukawa K, Furumoto S, et al. Correlations of (18)F-THK5351 PET with Postmortem Burden of Tau and Astrogliosis in Alzheimer Disease. Journal of nuclear medicine : official publication, Society of Nuclear Medicine. 2018;59:671–4.

[20]. Day GS, Gordon BA, Perrin RJ, Cairns NJ, Beaumont H, Schwetye K, et al. In vivo [(18)F]-AV-1451 tau-PET imaging in sporadic Creutzfeldt-Jakob disease. Neurology. 2018;90:e896–e906. [PubMed: 29438042]

[21]. Marquie M, Normandin MD, Meltzer AC, Siao Tick Chong M, Andrea NV, Anton-Fernandez A, et al. Pathological correlations of [F-18]-AV-1451 imaging in non-alzheimer tauopathies. Annals of neurology. 2017;81:117–28. [PubMed: 27997036]

[22]. Smith R, Wibom M, Pawlik D, Englund E, Hansson O. Correlation of In Vivo [18F]Flortaucipir With Postmortem Alzheimer Disease Tau Pathology. JAMA neurology. 2018.

[23]. Folstein MF, Folstein SE, McHugh PR. "Mini-mental state". A practical method for grading the cognitive state of patients for the clinician. J Psychiatr Res. 1975;12:189–98. [PubMed: 1202204]

[24]. Meltzer CC, Kinahan PE, Greer PJ, Nichols TE, Comtat C, Cantwell MN, et al. Comparative evaluation of MR-based partial-volume correction schemes for PET. J Nucl Med. 1999;40:2053–65. [PubMed: 10616886]

[25]. Lowe VJ, Lundt E, Knopman D, Senjem ML, Gunter JL, Schwarz CG, et al. Comparison of [(18)F]Flutemetamol and [(11)C]Pittsburgh Compound-B in cognitively normal young, cognitively normal elderly, and Alzheimer's disease dementia individuals. Neuroimage Clin. 2017;16:295–302. [PubMed: 28856092]

[26]. Jack CR Jr., Wiste HJ, Weigand SD, Therneau TM, Lowe VJ, Knopman DS, et al. Defining imaging biomarker cut points for brain aging and Alzheimer's disease. Alzheimers Dement. 2017;13:205–16. [PubMed: 27697430]

[27]. Raman MR, Schwarz CG, Murray ME, Lowe VJ, Dickson DW, Jack CR Jr., et al. An MRI-Based Atlas for Correlation of Imaging and Pathologic Findings in Alzheimer's Disease. J Neuroimaging. 2016;26:264–8. [PubMed: 27017996]

[28]. Mirra SS, Heyman A, McKeel D, Sumi SM, Crain BJ, Brownlee LM, et al. The Consortium to Establish a Registry for Alzheimer's Disease (CERAD). Part II. Standardization of the

neuropathologic assessment of Alzheimer's disease. Neurology. 1991;41:479–86. [PubMed: 2011243]

[29]. Murray ME, Dickson DW. Is pathological aging a successful resistance against amyloid-beta or preclinical Alzheimer's disease? Alzheimer's research & therapy. 2014;6:24.

[30]. Crary JF, Trojanowski JQ, Schneider JA, Abisambra JF, Abner EL, Alafuzoff I, et al. Primary age-related tauopathy (PART): a common pathology associated with human aging. Acta neuropathologica. 2014;128:755–66. [PubMed: 25348064]

[31]. Mackenzie IR, Neumann M, Bigio EH, Cairns NJ, Alafuzoff I, Kril J, et al. Nomenclature for neuropathologic subtypes of frontotemporal lobar degeneration: consensus recommendations. Acta Neuropathologica. 2009;117:15–8. [PubMed: 19015862]

[32]. Dickson DW, Bergeron C, Chin SS, Duyckaerts C, Horoupian D, Ikeda K, et al. Office of Rare Diseases neuropathologic criteria for corticobasal degeneration. Journal of neuropathology and experimental neurology. 2002;61:935–46. [PubMed: 12430710]

[33]. Hauw JJ, Daniel SE, Dickson D, Horoupian DS, Jellinger K, Lantos PL, et al. Preliminary NINDS neuropathologic criteria for Steele-Richardson-Olszewski syndrome (progressive supranuclear palsy). Neurology. 1994;44:2015–9. [PubMed: 7969952]

[34]. Ahmed Z, Bigio EH, Budka H, Dickson DW, Ferrer I, Ghetti B, et al. Globular glial tauopathies (GGT): consensus recommendations. Acta neuropathologica. 2013;126:537–44. [PubMed: 23995422]

[35]. Kosaka K, Yoshimura M, Ikeda K, Budka H. Diffuse type of Lewy body disease: progressive dementia with abundant cortical Lewy bodies and senile changes of varying degree--a new disease? Clin Neuropathol. 1984;3:185–92. [PubMed: 6094067]

[36]. McKeith IG, Boeve BF, Dickson DW, Halliday G, Taylor JP, Weintraub D, et al. Diagnosis and management of dementia with Lewy bodies: Fourth consensus report of the DLB Consortium. Neurology. 2017;89:88–100. [PubMed: 28592453]

[37]. Murray ME, Cannon A, Graff-Radford NR, Liesinger AM, Rutherford NJ, Ross OA, et al. Differential clinicopathologic and genetic features of late-onset amnestic dementias. Acta Neuropathologica. 2014;128:411–21. [PubMed: 24899141]

[38]. Robin X, Turck N, Hainard A, Tiberti N, Lisacek F, Sanchez JC, et al. pROC: an open-source package for R and S+ to analyze and compare ROC curves. BMC Bioinformatics. 2011 ;12:77. [PubMed: 21414208]

[39]. Perkins NJ, Schisterman EF. The Youden Index and the optimal cut-point corrected for measurement error. Biom J. 2005;47:428–41. [PubMed: 16161802]

[40]. Marquie M, Normandin MD, Vanderburg CR, Costantino IM, Bien EA, Rycyna LG, et al. Validating novel tau positron emission tomography tracer [F-18]-AV-1451 (T807) on postmortem brain tissue. Annals of neurology. 2015.

[41]. Josephs KA, Whitwell JL, Tacik P, Duffy JR, Senjem ML, Tosakulwong N, et al. [18F]AV-1451 tau-PET uptake does correlate with quantitatively measured 4R-tau burden in autopsy-confirmed corticobasal degeneration. Acta Neuropathol. 2016;132:931–3. [PubMed: 27645292]

[42]. Fillenbaum GG, van Belle G, Morris JC, Mohs RC, Mirra SS, Davis PC, et al. Consortium to Establish a Registry for Alzheimer's Disease (CERAD): the first twenty years. Alzheimer's & dementia : the journal of the Alzheimer's Association. 2008;4:96–109.

[43]. Kantarci K, Lowe VJ, Boeve BF, Weigand SD, Senjem ML, Przybelski SA, et al. Multimodality imaging characteristics of dementia with Lewy bodies. Neurobiology of aging. 2012;33:2091–105. [PubMed: 22018896]

Research in Context:

1. Systematic review: The authors reviewed the literature using traditional (e.g., PubMed) sources and meeting abstracts and presentations. The correlation of tau-PET imaging and autopsy in dementia cohorts has been performed in some small groups. These publications are appropriately cited.
2. Interpretation: Our findings demonstrate the contributions of tau-PET neuroimaging findings to diagnosis and demonstrate the impact of antemortem imaging findings.
3. Future directions: The manuscript suggests possible improvement in pathological and imaging data techniques and analyses that could be considered to improve correlations.

   Examples include further understanding: (a) larger study groups with tau-PET and autopsy, (c) development and inclusion of new, specific neurodegenerative imaging biomarkers and (b) inclusion of visual interpretation of neuroimaging data.

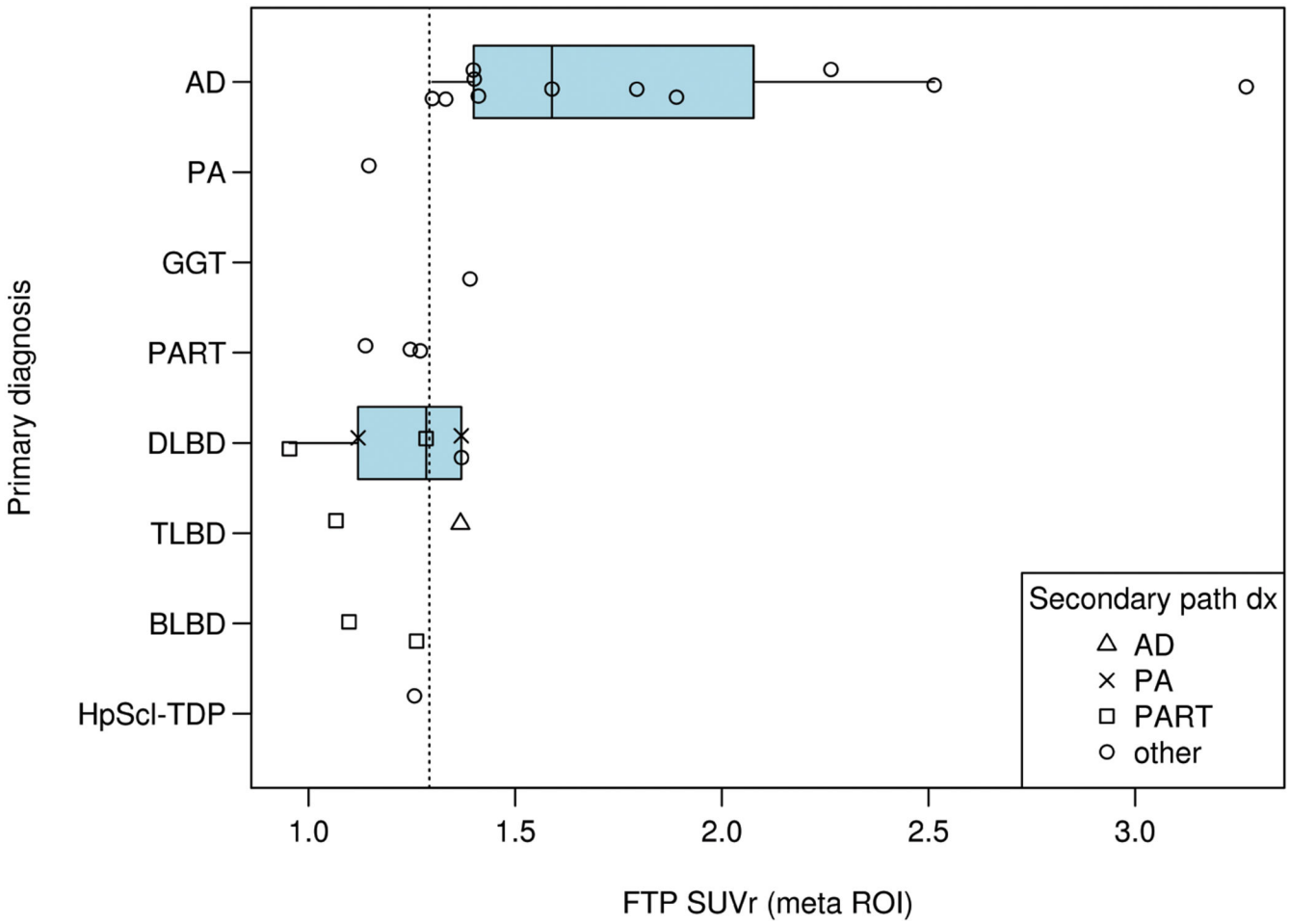

Figure 1. SUVr by Different Primary Neuropathologic Diagnoses.

FTP-PET SUVr using the meta ROI is shown on the x-axis relative to the different primary neuropathologic diagnoses on the y-axis. Each participant's secondary neuropathologic diagnosis shown in the right lower callout with different shapes indicating the secondary diagnoses. The vertical dotted line represents the SUVr value of 1.29. A two-sample t-test suggested that ADs had more SUVr load on average (mean FTP SUVr) than LBD (1.83 to 1.21, p=0.008).

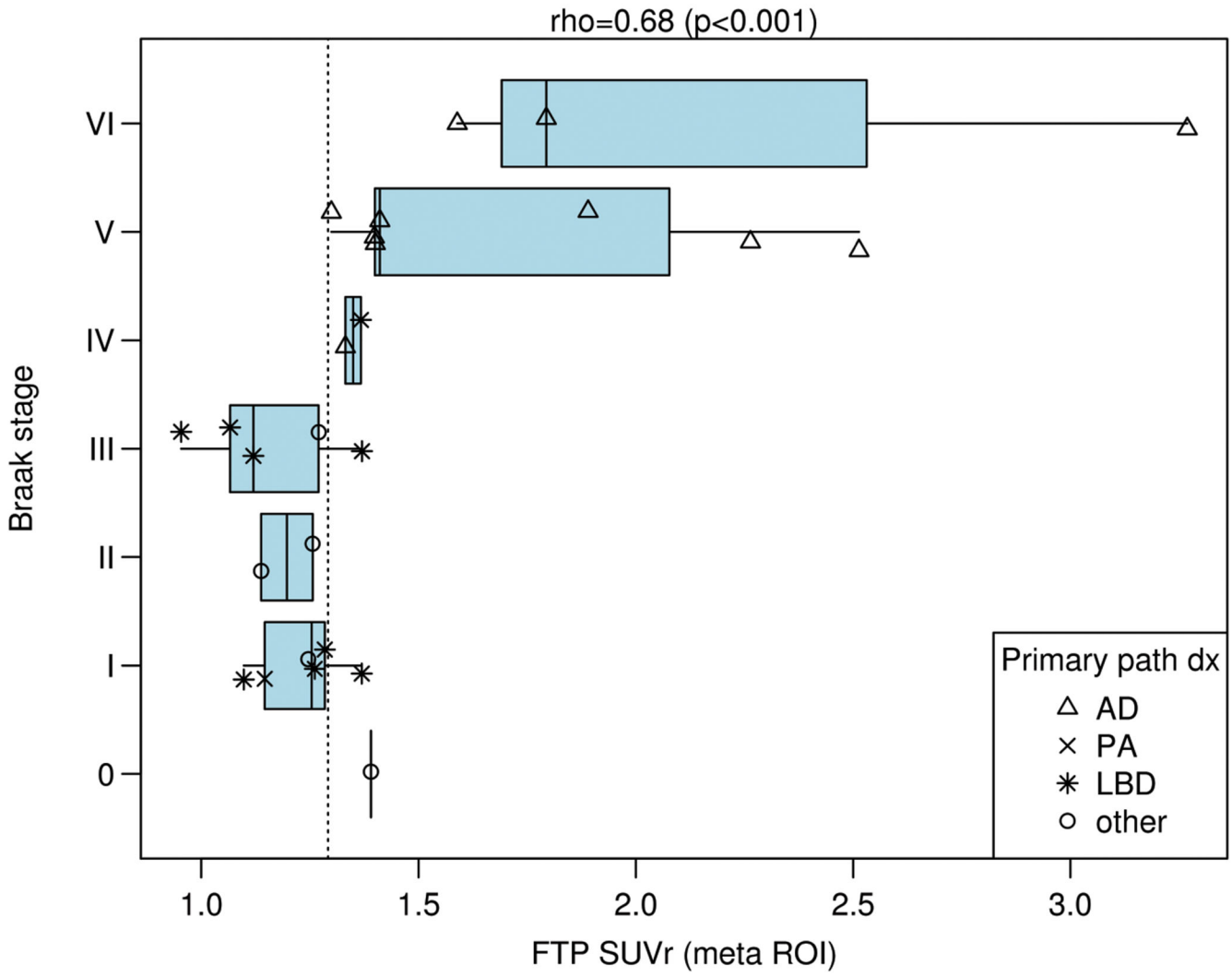

Figure 2. SUVr by Braak NFT Stage.

FTP-PET SUVr using the meta ROI is shown on the x-axis relative to the Braak NFT stage on the y-axis. Each participant's primary neuropathologic diagnosis is shown in the right upper callout with different shapes indicating the secondary diagnoses. The vertical dotted line represents the SUVr value of 1.29. Only the AD group approached significance for subgroup correlation with Braak stage (p=0.13) but low participant numbers by subgroups were likely a limitation. After adjusting for time from imaging to death, the partial Spearman's rank correlation between Braak and TAU SUVR is unchanged at 0.67 with 95% confidence interval (CI) (0.34, 0.85) vs. 0.68 (95% CI: 0.40, 0.85) when unadjusted.

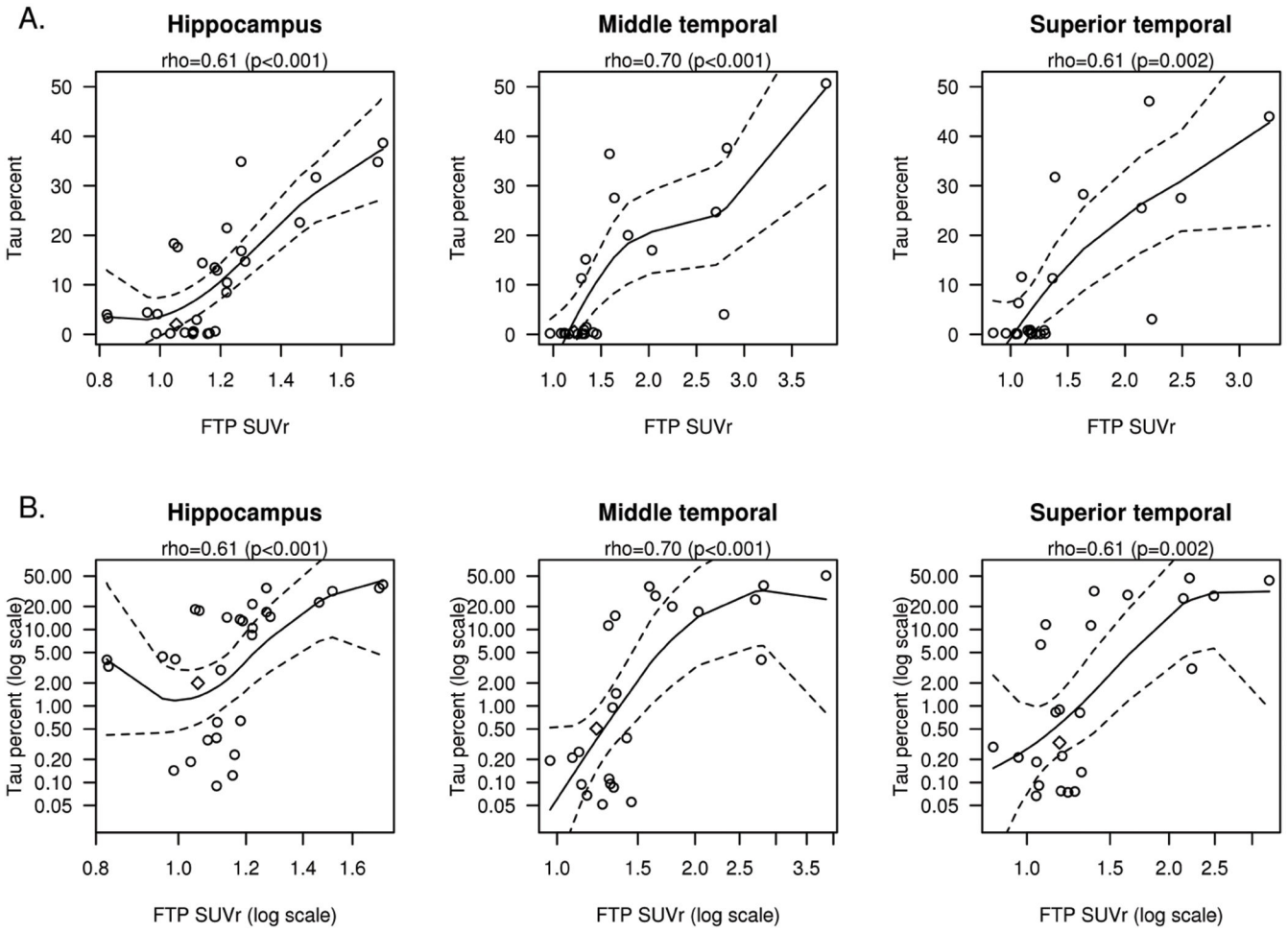

Figure 3. Correlations between %Tau Burden and SUVR.

FTP-PET SUVr correlation to the % tau burden measured on immunohistochemistry is shown for the hippocampus, middle temporal, superior temporal ROIs (A). The x and y axes are also shown in log scale (B) to better demonstrate the tau-PET SUVr values with low percentage tau burden regions. Includes local regression curves (black) with 95% confidence band (dashed lines). The AGD participant is shown with a diamond shape.

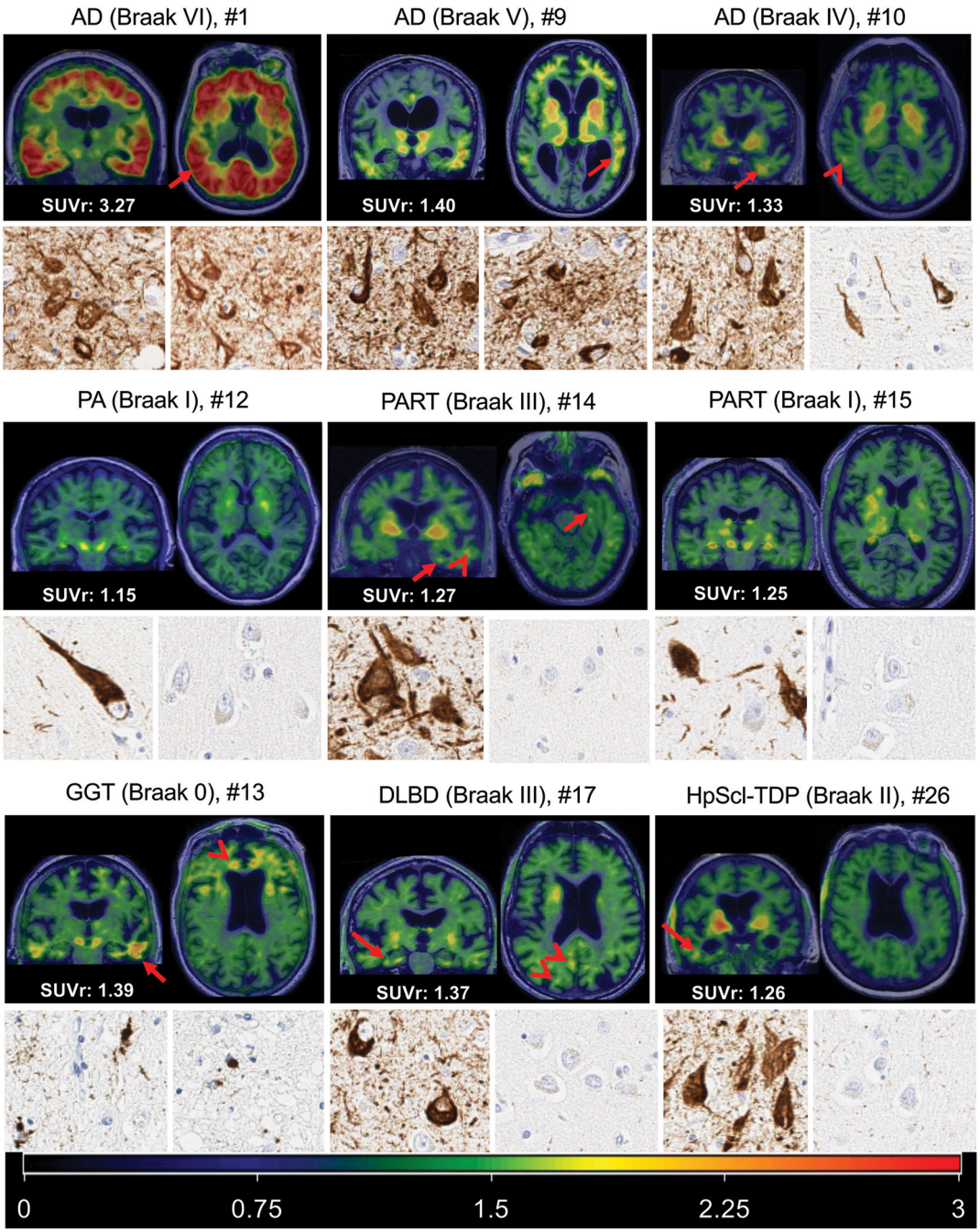

Figure 4. FTP-PET images and corresponding histology in AD, Pathological Aging, PART, GGT, DLBD, and Hippocampal Sclerosis.

Coronal and axial images are show for each participant registered to their own MRI. The SUVr value for each is shown in the bottom left of each respective set of images and visually elevated focal uptake (greater than background) is described. The representative color scale with SURr values is shown in the bottom panel. Below the FTP-PET images is a 10x magnification for each participant of the transentorhinal cortex and middle temporal cortex. The AD examples show elevated FTP-PET signal (arrows) corresponding to Braak tangle stage. In the Braak IV AD participant, subtle FTP-PET signal in the posterior

temporal region (arrowhead) is also seen. The participant with PA (middle left) had a non-elevated SUVr (1.15) with no visible FTP-PET signal in the entorhinal cortex or temporal lobes. The participant with PART and Braak III (middle row, center) had a non-elevated SUVr (1.27) with visible FTP-PET signal in the entorhinal/temporal gyrus (arrows) and lateral temporal lobe (arrowhead). The participant with PART and Braak I (middle right) had a non-elevated SUVr (1.25) without visible FTP-PET signal. The GGT participant had elevated focal tau accumulation in temporal (arrow) and frontal lobes (arrowhead). The participant with DLBD (lower row, middle), had elevated FTP-PET signal in temporal (arrow), posterior cingulate and parietal-occipital regions (arrowheads). FTP-PET signal is focally elevated in the hippocampal sclerosis participant (bottom row, right) in the right inferior temporal region which was not the side evaluated at autopsy. The AD examples show reduction in tau burden on histology from left to right most notably in the temporal tissue sample. The middle row of low Braak participants show no middle temporal gyrus tau and greater transentorhinal tau burden in the PART Braak III tissue. In the bottom row, globular oligodendroglial inclusions were found in the cortex of the GGT participant, but not neurofibrillary tangle pathology. Neurofibrillary tangle pathology was observed in the transentorhinal region in both DLBD and HpScl-TDP participants with minimal neuritic pathology observed in the middle temporal cortex of DLBD and none found in the HpScl-TDP participant.

Table 1.

Demographics by Neuropathology Diagnosis

Demographics	AD (n=11)	PA (n=1)	GGT (n=1)	PART (n=3)	DLBD (n=5)	TLBD (n=2)	BLBD (n=2)	HS-TDP (n=1)	Total (n=26)
Sex									
Female	5	1	1	0	1	0	1	1	10
Male	6	0	0	3	4	2	1	0	16
Education									
Mean (SD)	16 (2.1)	13	16	13 (5.6)	16 (3.0)	13 (1.4)	15 (3.5)	14	15 (2.8)
Age at Scan, (years)									
Mean (SD)	78 (12.0)	68	65	86(16.0)	76 (10.5)	88 (0.6)	83 (3.6)	86	79 (11.2)
Scan to Death (months)									
Mean (SD)	15.1 (6.6)	10.9	20.4	15.5 (8.0)	18.5 (9.5)	6.1 (5.0)	11.0 (7.0)	8.4	14.6 (7.3)
Range	7.1 - 26.2			9.2 - 24.5	6.5 - 29.8	2.5 - 9.6	6.0 - 16.0		2.5 - 29.8
APOE ε4, no.									
No	6	0	0	3	4	1	1	1	16
Yes	5	1	1	0	1	1	1	0	10
MMSE[1]									
Mean (SD)	18 (8)	29	24	27 (2)	22 (6)	28 (1)	26 (4)	21	**22 (7)**
GMWM PVCN PiB SUVr[2]									
Mean (SD)	2.72 (0.81)	1.67	1.65	1.39 (0.02)	1.57 (0.30)	1.83 (0.72)	1.39 (0.22)	1.36	2.01 (0.80)
Range	1.80 - 4.66			1.37 - 1.41	1.21 - 2.02	1.32 - 2.34	1.23 - 1.55		1.21 - 4.66
GMWM PVCN FTP SUVr[3]									
Mean (SD)	1.83 (0.62)	1.15	1.39	1.22 (0.07)	1.22 (0.18)	1.22 (0.21)	1.18 (0.12)	1.26	1.48 (0.51)
Range	1.30 - 3.27			1.14 - 1.27	0.95 - 1.37	1.07 - 1.37	1.10 - 1.26		0.95 - 3.27

[1] MMSE were missing in 8 of the group at the time of the imaging visit as they were unable to be tested due to disease severity. In these participants the most proximal prior available MMSE was then used.

[2] Voxel size weighted average of uptake in gray and white matter (GMWM) regions prefrontal, orbitofrontal, parietal, temporal, anterior and posterior cingulate, and precuneus scaled by weighted average of cerebellar crus 1 and 2 without partial volume correction (PVCN).

[3] Voxel size weighted average of uptake in GMWM regions entorhinal, amygdala, parahippocampal, fusiform, inferior and middle temporal scaled by weighted average of cerebellar crus 1 and 2 without PVCN.

Acronyms: AD – Alzheimer's disease, BLBD – brainstem Lewy body disease, DLBD – diffuse Lewy body disease, GGT – globular glial tauopathy, HS-TDP – hippocampal sclerosis of a TDP-43 etiology, NA – not available, MMSE – mini-mental state examination, PA – pathological aging, PiB – Pittsburgh compound B, PVCN – partial volume correction no, SD – standard deviation, $SUVr$ – standard value uptake ratio, TLBD – transitional Lewy body disease.

Table 2.

Individual Participant Data

Participant	Sex	Clinical Dx	Primary Pathologic Dx	Secondary Pathologic Dx	Tau, SUVr*	Thal	Braak	Neuritic Plaques	Scan to Death (mos)
1	F	Probable AD	AD	DLBD	3.27	4	VI	Frequent	20.4
2	M	Probable AD	AD	CAA	2.51	5	V	Sparse-Moderate	22.4
3	F	PCA	AD	DLBD	2.26	5	V	Moderate-Frequent	14.4
4	M	Probable AD	AD	ALB	1.89	5	V	Moderate	10.7
5	F	CBS	AD	None	1.79	5	VI	Frequent	9.8
6	M	lvPPA	AD	ALB	1.59	5	VI	Moderate	11.7
7	M	MCI	AD	VaD	1.41	5	V	Sparse-Moderate	7.1
8	F	Dementia≠	AD	HpScl-TDP	1.40	5	V	Moderate-Frequent	10.5
9	M	lvPPA	AD	Melanoma	1.40	5	V	Frequent	10.1
10	M	Probable AD	AD	TLBD	1.33	5	IV	Moderate	22.7
11	F	MCI	AD	DLBD	1.30	5	V	Frequent	26.2
12	F	Normal	PA	None	1.15	3	I	None	10.9
13	F	bvFTD	GGT	HpScl-TDP	1.39	3	0	None	20.4
14	M	Normal	PART	None	1.27	1	III	None	9.2
15	M	Normal	PART	SAH	1.25	0	I	None	24.5
16	M	Normal	PART	None	1.14	1	II	None	12.9
17	M	PD	DLBD	SC	1.37	3	III	None	11.6
18	M	DLB	DLBD	PA	1.37	3	I	Moderate	6.5
19	M	DLB	DLBD	PART, definite	1.28	0	I	None	29.8
20	F	Normal with RBD	DLBD	PA	1.12	3	III	Sparse	24.6
21	M	DLB	DLBD	PART, definite	0.95	0	III	None	19.9
22	M	Normal	TLBD	AD	1.37	3	IV	Moderate	2.5
23	M	Normal	TLBD	PART, probable	1.07	1	III	None	9.6
24	F	Normal	BLBD	PART, definite	1.26	0	I	None	6.0
25	M	Normal	BLBD	PART, probable	1.10	1	I	None	16.0
26	F	Prob AD	HpScl-TDP	AGD	1.26	1	II	None	8.4

Acronyms: Dx – diagnosis, SUVr – standard uptake value ratio, mos – months, F – female, M – male, MCI -mild cognitive impairment, AD – Alzheimer's disease, IvPPA – logopenic variant of primary progressive aphasia, PCA – posterior cortical atrophy, CBS – corticobasal syndrome, bvFTD – behavior variant frontotemporal dementia, PD – Parkinson's disease, DLB – dementia with Lewy bodies, RBD – REM behavior disorder, PA – pathological aging, GGT – globular glial tauopathy, PART – primary age-related tauopathy, DLBD – diffuse Lewy body disease, TLBD – transitional Lewy body disease, BLBD – brainstem Lewy body disease, HpScI – hippocampal sclerosis, TDP -TAR DNA binding protein, VaD – vascular disease, ALB – amygdala predominant Lewy bodies, CAA – cerebral amyloid angiopathy, SAH – subarachnoid hemorrhage, SC – senile change, AGD – argyrophilic grains disease.

[*] Tau SUVr derived from meta-ROI;

[≠] Dementia hard to classify

Alzheimers Dement. Author manuscript; available in PMC 2021 March 01.